Parametric study of adhesive joints with non-flat sinusoid interfaces

S.M.J. Razavi*, F. Berto, M. Peron, J. Torgersen

Department of Mechanical and Industrial Engineering, Norwegian University of Science and Technology (NTNU), Richard Birkelands vei 2b, 7194, Trondheim, Norway.

Abstract

The role of sinusoid interface shape on the stress distribution and load bearing capacity of the adhesively bonded single lap joints has been investigated numerically and experimentally. The experimental results showed that the interface non-flatness can considerably influence the adhesive joint strength and this was in correlation with the numerical results obtained from finite element analysis. Parametric studies were conducted using finite element method to investigate the role of various wave heights, wave lengths, adhesive thicknesses and also mechanical properties of adhesives and adherends on the stress distributions of the bonded joints. Lower wave lengths and higher wave height resulted in decreased peak stresses in the mid-line of the adhesive layer and consequently increase the strength of the joint. Besides, the lower adhesive thickness and lower stiffness ratio of adherends and adhesive caused an increase in the efficiency of the non-flat single lap joints.

Keywords: adhesively bonded joint; interface profile; stress analysis; failure; single lap joint

* Corresponding author
Email: javad.razavi@ntnu.no (S.M.J. Razavi)

1- Introduction

Adhesive bonded joints have attracted considerable attention in various industries such as marine and aerospace as a replacement for traditional joining methods including riveting, bolting and welding. Based on manufacturing considerations, single lap joints (SLJ) seem to constitute the easiest and cheapest type of adhesively bonded joints and welded joints [1-3]. However, the offset of the two sheets in SLJs causes a misalignment and results a bending moment in the joint which intensifies the local stresses at both ends of the lapped region and leads to an inefficient load transfer [4-6]. The ends of adhesive layer in single lap joint are the weakest areas which often fail due to the normal local stresses. Several studies have been conducted in recent years about single lap joints to provide ideas and solutions in order to improve the joint strength [7-10]. Improving the joint strength, by reducing peel and shear peak stresses at critical areas can be obtained by two methods, modifications of adhesive materials (e.g. incorporating nano, micro and macro particles and fibers into the neat adhesive [11-16] and application of functionally graded adhesives [17-19]) and modifying the geometry of the joint. Different methods were proposed by scholars for modification of the adhesive joint geometries including chamfering or beveling and hole drilling of the adherends [20-22]. Introducing local compressive stresses at both ends of adhesive layer was the aim of some researchers which led to design of non-flat adhesive joints. Three main geometries of non-flat adhesive joints are illustrated in Fig. 1 including the reverse bent, wavy and sinusoid interface single lap joints. A short description of previous researches related to this kinds of adhesive joints is given in the following part.

Boss et al. reported that modifying the shape of adherents can reduce the peak values of shear and peel stresses in SLJ which can improve the overall strength of the joint [23]. This result is the same as that presented by McLaren [24]. McLaren et al. suggested simply deforming the substrate at the

end of the overlap length to improve the stress distribution within the overlap area of single lap joints (Fig. 1a). The new geometry of single lap joint was named reverse-bend SLJ which produces a bending moment in the adherends opposite to that occurring in the conventional single lap joint. The reverse moment diminishes the maximum peel stress and leads to a fairly uniform shear stress in the bond line. Fessel et al. applied the reverse-bent geometry to composite adherends and compared the behavior of the reverse-bent joint with the traditional SLJ configuration using some numerical and experimental investigations. It was reported that the value of failure load enhancement in reverse-bent joint depends upon the chosen material combination [25]. Additionally, Fessel et al. investigated the fatigue behavior of reverse-bent joints using substrates with different yield and plastic deformation characteristics. They reported that the enhancements obtained under static loading conditions translate to even higher benefits in fatigue loading [26]. The efficiency of reverse-bent joints made of brittle and ductile adhesives were evaluated by Campilho et al. using both numerical analysis and experiments [27]. Results showed a major improvement of joint strength for the brittle adhesive, but the joints with the ductile adhesive were not much affected by the bending technique. You et al. investigated the effect of different preformed deflection angles in reverse-bent SLJs on improvement of the joint strength [28]. According to their experimental results, the highest value of the average ultimate load of SLJs was obtained when the preformed angle was equal to 7^{o} (about 64% higher than the standard flat SLJ). Zeng and Sun proposed a new geometry of single lap joint namely wavy lap joint (Fig. 1b) [29,30]. The maximum peel stress at two ends of adhesive layer in wavy lap joint was lower than that of flat single lap joint. Lower maximum stresses at adhesive layer caused enhancement of load bearing of the joint. Moreover, they performed comparative fatigue tests on the wavy lap joints to assess the effect of adherend non-flatness on the fatigue life of the joint [31,32]. According to their

test results, the wavy lap joint had a much longer fatigue life than the conventional lap joint. Avila and Bueno conducted experimental and numerical studies on single-lap joints with wavy geometry using composite adherends; the result of which, showed that application of adherends with wavy shapes increased the strength of the joints nearly 40% with respect to the conventional SLJ [33]. Shiva Shankar et al. also reported strength enhancement in wavy SLJs [34]. In another research, Fessel compared the stress distribution of the reverse-bent and the wavy joints, with the stresses of the traditional single lap joint [35]. They found that the single lap joints failed mostly due to the peel stress and yielding of the substrates, whereas the reverse-bent joints mostly failed in shear or due to lateral straining of the substrates away from the overlap.

Increasing the roughness of adherends surface before applying the adhesive is one common practice to improve mechanical locking and adhesion at the interface of adhesive and adherends [36-39]. However, according to the small dimensions of the surface roughness, it doesn't significantly influence the load transfer mechanics. Ashrafi et al. studied the feasibility of improving the structural performance of single lap joints by varying interface shape but not overall joint envelope. They tested two different geometries of SLJs with sinusoid interfaces made of glass fiber reinforced polymer (Fig. 1c). It was reported that the interface non-flatness has significant effect on the mechanical behavior and strength of the bonded joints [40]. Razavi et al. investigated the mechanical behavior of SLJs made of non-flat zigzag adherends. They found that according to the geometry of the interlocking teethes, the load bearing capacity of the joint can be increase or decrease [41].

Non-flattening the adherends in the adhesively bonded joints can be considered as an efficient technique for improving the mechanical behavior of the adhesive joints. The substrates can be prepared by various interface geometries. As already stated, the non-flat sinusoid interfaces have

been recently studied by Ashrafi et al. [40], however, the reported results are related to composite adherends and a limited numbers of geometries and design parameters. In this paper, the efficiency of non-flattening the interface of metal-adhesive SLJs is evaluated by considering different key parameters including the wave length, the sign of the wave slope, the wave height, the adhesive thickness and mechanical properties of adherends and adhesives. This paper aims to examine the effects of different interface morphologies on the distribution of shear and peeling stresses, particularly their maximum values and joint-strength of adhesively bonded joints through experimental investigations and numerical modelling. For this purpose, about twenty different configurations of adhesive interface geometries were considered for numerical investigations.

2- Experiments

To investigate the effects of interface non-flatness on the strength of the single lap joints, single lap joints made of aluminum 7075-T6 substrates bonded with a two-component epoxy paste adhesive named Araldite® 2015 were made. Some standard tensile tests were conducted to obtain the stress-strain curve of both adherends (ASTM E8 [42]) and adhesive base (ASTM D638 [43]) (see Fig. 2). Five specimens from each material were tested in room temperature and under constant tensile rate of 1 mm/min and the results are given in Table 1. The substrates were cut from 12.5 mm thick sheets using wire cut CNC machine. Fig. 3 shows the geometrical dimensions of adhesive joints. The overlap length L, the thickness of bond line t, the substrate thickness H and the substrate free length were 30, 0.2, 5 and 45 mm, respectively. Also the value of wave height, A was equal to 1.5 mm for all of specimens. It can be observed that the outer envelope of SLJs with sinusoid interface is the same as that with a flat interface.

In this paper, each adhesive joint is named by a short name which is consist of three part S(B)±, first part is the S for sinusoid interfaces; the second part, B indicates the wave length and the third part is the sign of the wave slope (dy/dx) at x = 0. For example the S(L/2)+ joint is a sinusoid adhesive joint with wave length of L/2 (i.e. the interface has 2maximum peaks and two minimum peaks) and positive wave slope dx/dy > 0. Five different single lap joints with various interface shapes were considered for the experiments (see Fig. 4). The wave lengths were considered as L and L/2, with both negative and positive wave slopes at x = 0. Subsequently, for all the specimens, the substrates were pre-treated prior to bonding. The pre-treatment consisted of a first wash by the acetone followed by an acid etch according to DIN 53281 standard [44] to maximize environmental confrontation and bonding strength. The ingredients of the etching solution are presented in Table 2. The aluminum adherends prepared for the adhesive supplement are illustrated in Fig. 4.

The sinusoid interface profile in Cartesian coordinate system is defined as

$$y = A\sin(2\pi x / \lambda) \tag{1}$$

where A is the wave height which can be positive or negative according to the bond line slope at x = 0 and λ is the wavelength. Two adherends of the same shape are required to make a bond with non-flat interface. After applying the adhesive layer, the adherends were separated by a vertical distance of t = 0.2 mm that was constant along the bonding length and it was applied using a manufacturing fixture. It is worth mentioning that the when two sinusoid adherends with the same geometry are used for joint fabrication, the resulting gap width, t' is not constant. Fig. 5 illustrates a schematic of bond line indicating both adhesive thickness, t and gap width, t'.

Considering a segment of arc whose length is Δs. For small values of Δy and Δx, the approximate length of Δs is given by the Pythagorean theorem,

$$\Delta s \approx \sqrt{\Delta x^2 + \Delta y^2} \tag{2}$$

Substituting the infinitesimals *dx* and *dy*, results

$$\frac{ds}{dx} = \sqrt{1 + \left(\frac{dy}{dx}\right)^2} \tag{3}$$

According to Fig. 5, two triangles Δ*ABC* and Δ*abc* are similar because the corresponding angles have the same measure, thus, the lengths of corresponding sides are proportional.

$$\frac{ds}{dx} = \frac{t}{t'} = \sqrt{1 + \left(\frac{dy}{dx}\right)^2} \tag{4}$$

Hence the gap width between two adherends can be calculated as bellow

$$t' = \frac{t}{\sqrt{1 + \left(\frac{dy}{dx}\right)^2}} \tag{5}$$

According to Eq. 5, the gap between adherends equals adhesive thickness only where the bond slope is zero ($dy/dx = 0$) otherwise it would be less. For example, for a given wave height of A = 1.5 mm and wavelength of λ = 15 mm, the maximum value of bond slope is 0.63 which results a gap width of $t' = t/1.18$. The adhesive joints were cured for seven days at room temperature (about 25^{o}C). Five different types of adhesively bonded joints, namely non-flat and flat SLJ, were tested under static loading to obtain the failure load and compare the results with that of obtained from numerical stress analysis. Five samples for each specimen configuration were tested under a displacement control static loading at a rate of 1 mm/min and the related load levels were recorded.

3. Finite Element Model

In this research, two-dimensional analyses of single lap joints with different interface shapes were performed using the ABAQUS software. Applying the tensile load to the single lap joint causes both tension and bending of the joint, resulting shear and peel stresses in the adhesive layer. Finite element simulations of simplified two-dimensional models of sinusoidal interfaces with isotropic adherends were carried out to obtain the distribution of shear and peel stresses along the bond line. Parametric variations were studied via FEA to highlight the role of interface shape on the distribution of stresses and inherently, the overall strength of the bonded joints. The stress analyses were investigated considering the isotropic linear elastic properties of the adhesive and adherends. The geometric dimensions used for finite element simulation are provided in Fig. 2. An important point in designing the non-flat interface joints is the slope of two ends of the bond line (dy/dx) which can be positive or negative. Thus, for all six specimens with specific wave lengths, two different conditions of positive and negative slopes of bond line were considered (see Fig. 6). Additionally, the effect of the wave height, the adhesive thickness and the elastic modulus of adhesive base and adherends were assessed using finite element analysis.

Two dimensional finite element analyses were carried out to simulate the behavior of the adhesive joints. The 8-node biquadratic quadrilateral reduced integration elements were used for this purpose. A mesh convergence study was also conducted to obtain the appropriate element size for stress analyses. Eight elements were considered in the adhesive thickness to obtain the distribution of stress in the adhesive layer. The element sizes used for adherents meshing were with a pattern that became coarser by getting away from the bonding location. Fig. 7 shows a typical element size in finite element model. The models were collapsed at one end, while the other end of the joint was allowed to translate only in axial direction without rotation. An axial tensile load equal to 1 MPa was applied at the end of the joints.

In order to obtain the peel and shear stresses along the mid-plane of bond line, the equations 6 and 7 were employed [45].

$$\sigma_n = \sigma_x \sin^2\theta + \sigma_y \cos^2\theta - 2\tau_{xy} \sin\theta\cos\theta \quad (6)$$

$$\sigma_s = -(\sigma_x - \sigma_y)\sin\theta\cos\theta + \tau_{xy}(\cos^2\theta - \sin^2\theta) \quad (7)$$

where σ_x, σ_y, τ_{xy} are adhesive stresses in global coordinates and $\theta = \arctan(dy/dx)$ is the slope angle of the bond line. Numerous finite element analyses with consideration of material and geometry nonlinearities were conducted on the tested adhesive joints. The numerical results showed a negligible plastic strain near the bimaterial conjunction of adherends only in S(L/2)-specimen. The numerical part of this research aims to show only the benefit of different interface geometries by comparing like-for-like stress distributions.

4. Result and Discussion

4.1. Experimental Results

It is worth mentioning that the local moments on both ends of adhesive layer result the peel and cleavage stresses which can lead to reduction of adhesive joints strength. These normal stresses typically lead to failure of the adhesive joints before the shear stress is fully developed so that the nominal maximum joint strength is not attained. Additionally, the local bending moments may result in yielding of the adherends, which may also limit the joint strength. Thus, the peel stress/strain should be considered as a key parameter in design of adhesively bonded joints. Fig. 8 illustrates local stresses at both ends of adhesive layer. According to the Fig. 8, adherend non-flatness can change the stress condition in the adhesive joint specially altering the values of peak stresses at both ends of bond line. Negative and positive bond line slope create local compressive

and tensile stresses in adhesive layer. Presence of local compressive/tensile stresses at critical points of bond line reduces/increase the peak values of peel stress and shear stress in adhesive layer which leads to enhancement/reduction of load bearing of the joint. In the case of symmetrical interface geometry, similar local stresses will occur on both ends of adhesive layer.

The typical load-displacement curves of single lap joints with sinusoid and flat interfaces are shown in Fig. 9. The numbers marked on the curves denote schematic view of the typical specimen at each stage of loading (Fig. 9b). Fig. 9b illustrates the progressive failure in the adhesive layer obtained from experimental results. The bold lines on the images indicate undamaged regions of adhesive layer at each stage of deformation. According to Fig. 9, five types of SLJs differ significantly in their mechanical behavior.

For the S(L)+ and S(L/2)+ specimens, the final failure of the joints occurred at approximate loads of 5800 N and 4700 N, respectively which are 30% and 43% lower than flat joints . However for S(L)- and S(L/2)- specimens, the final failure occurred at a load around 11000 N and 12500 N which are 33% and 51% higher than the values obtained from flat joints. It should be noted that flat-joint average shear strength is approximately 22MPa.

The failure load of sinusoid joints with positive slope (S(L)+ and S(L/2)+) was significantly lower than flat SLJs. Unlike the other tested joints, the load-displacement curves of SLJs with positive bond line slope were not smooth which is due to the local failure of adhesive layer at both ends of bond line (see Fig. 9b). After crack nucleation and propagation on both sides of the bond line (point 2), the crack is arrested in the bond line and adhesive joint still sustain the tensile loading. Finally, increasing the applied load leads to sudden fracture of adhesive joint (point 3 for the joint S(L)+). On the other hand, sinusoid joints with negative bond slope had higher load bearing capacity compared to flat SLJs. Existence of local compressive stresses at both ends of adhesive layer in

sinusoid joints with negative bond slope (S(L)- and S(L/2)-) improved the joints strength. For S(L/2)- joints, crack initiation occurred from the interior waves. Fig. 10 presents comparative experimental results of failure loads obtained for single lap joints with different interface geometries.

4.2. Results of Parametric Studies

In order to compare the stress conditions of different interface geometries, the maximum value and the uniformity of the stress distribution were compared. The stress distribution for the joint with even numbers of waves in the interface is quite different when the bond line slope is positive or negative. As shown in the coming figures, the stress distribution for the negative slope of the bond line is much lower than the values for the positive slope of the bond line. For every specimen the maximum peel stresses are generally higher than the maximum shear stresses, so this indicates that the adhesive joints failure is mainly a result of the peel stress and initiates from where it has the maximum value (i.e. bonded joint edge).

During investigation of the stress distribution in the middle of adhesive thickness, a path was considered in the mid-line of adhesive layer and the stresses were obtained on the aforementioned path. Figs. 11 and 12 show the distribution of adhesive peel and shear stresses along the joint midlines as a function of normalized distance from the bond line tip (x/L). The resulting stresses are normalized by the applied axial stress. The maximum values of peel and shear stresses occur at the edge of the joint for all different configurations.

According to Figs. 11 and 12, for models with antisymmetric interface shapes (with respect to the mid length (x/L=0.5) of the bond line), the stress distribution has a symmetric condition (Figs. 11

and 12 - (b), (d), and (f)), whereas for models with symmetric interface shapes, the stress contours have an asymmetric distribution (Figs. 11 and 12 - (a), (c), and (e)). This asymmetric stress condition causes the stress values to lack uniformity with bias in one side of the adhesive layer. This leads to a more critical condition for the adhesive joint because the crack nucleates from the bias side with higher stress value. Although the peel stress is the determinative parameter in failure of the adhesive joints; however, an increment of the maximum value of shear stress makes the stress condition more crucial.

According to Figs. 11 and 12 - (a), (c), and (e), the maximum peel/shear stress of sinusoid joints at one end of the adhesive joint has become more than the value of peel stress for the flat joints, so using the sinusoid interfaces with symmetric interface (for both positive and negative wave slope $dy/dx>0$, $dy/dx<0$) had the negative effect on the stress uniformity and did not reduced the maximum value of the peel/shear stress in the adhesive layer. It should be noted that for SLJs with symmetric interface, failure initiates from the bias side with higher stress value.

Considering Figs. 11 and 12 - (b), (d), and (f), the maximum peel/shear stress value at both ends of the joint with antisymmetric interface had the same value. For the antisymmetric interface joints with positive slope of the bond line at x = 0 ($dy/dx > 0$) (S(L)+, S(L/2)+, and S(L/3)+), the maximum peel/shear stress was increased, whereas for the joints with negative bond line slope ($dy/dx < 0$) (S(L)-, S(L/2)-, and S(L/3)-), the maximum peel/shear stresses were decreased. Details of maximum peel and shear stresses for different SLJ configurations are given in Table 3.

According to the twelve different configurations of adhesive sinusoid interface, the best peel/shear stress distributions resulted for the joints with antisymmetric interface and negative slopes of adhesive bond line ($dy/dx < 0$). The reduction of maximum peel stresses for two cases of S(L/2)- and S(L/3)- were almost the same and it was about 41%. Moreover, the reduction of maximum

shear stress for the adhesive joints of S(L/2)- and S(L/3)- were respectively, 43% and 34%. This shows quite an acceptable reduction value which is in line with the failure load enhancements obtained in the experimental part of this research. Generally, the non-flat interfaces had the same but not equal effect on the maximum values of peel stress and shear stress. Although the SLJs with sinusoid interfaces had improvement in stress condition, the number of sinusoid geometries which lead to a more uniform stress distribution is limited. According to the data provided in Table 3, only for three cases (S(L)-, S(L/2)- and S(L/3)-) the peak value of peel/shear stresses was decreased.

The other parameter that can play an important role in the efficiency of SLJs with non-flat interfaces is the wave height. The value of wave height, A was considered equal to 1.5 mm in previous results. Here, nine different values of normalized wave height, A/H is considered for stress analysis including positive, zero, and negative wave heights. Figs. 13 and 14 illustrate the peel stress and shear stress distribution along the bond line of SLJs with sinusoid interface for wave length of (L/2). According to the Figs. 13 and 14, higher wave heights results in intensifying the effect of adherends non-flatness. For negative higher normalized wave height, the stress reduction was increased and this was a result of better mechanical locking between two sinusoid adherends. For example the stress reduction for the sinusoid joint with A/H = -0.2 the peel stress is about 16% lower than flat joint, while for the joint with A/H = -0.5, the peel stress reduction is almost 49%. It is worth mentioning that increasing the wave height has a practical limit. Increasing the normalized wave height leads to a reduction in the adherend ligament size and this results higher tensile stresses in adherends. Higher tensile stresses in adherends may cause an undesirable elongation or in a worse case, the adherend failure. The details of effect of wave height on stress distribution of SLJs are provided in Table 4. According to the results given in Table 4, increasing

the wave height from A/H = -0.5 to A/H = -0.6 reduced the peel stress reduction from 49% to 36%, this may be a reason of reduction of adherend overall stiffness. Additionally, by increasing the wave height and consequently reducing the adherend ligament, the load bearing of first and last waves on the adherend is reduced and because of deformation in ligament, the load is dominantly transferred by two middle waves. This causes the maximum peel/shear stress to occur in the middle of the joint. However, for the joint with A/H = -0.2 and -0.3 the location of maximum peel/shear stress is at two ends of the joint.

Reducing the distance between to adherends can lead to an improved mechanical locking between two adherends. This subject was assessed by analyzing single lap joints with both flat and sinusoid interfaces and different values of adhesive layer thickness, t. Four different values of adhesive layer thickness were considered for finite element analysis including t = 0.1, 0.2, 0.5 and 1 mm. It should be noted that the wave length and wave height was constant in these analyses. Details of FE results are given in Table 5. It can be concluded that lower adhesive thicknesses increases the efficiency of sinusoid joints. The maximum peel stress in sinusoid joint with t = 1 mm is 23% lower that flat joint with same adhesive thickness. However, the maximum peel stress in sinusoid joint with t = 0.1 mm is 45% lower than flat joint with same bond line thickness.

A comparative results of the maximum peeling and shear stresses in the bonded joint for bonded joints with different stiffness ratio of adherends and adhesives are provided in Table 6. The maximum peeling and shear stress reductions increase (in a relatively linear manner) by decreasing the stiffness ratio ($E_{\text{adherends}}$ / E_{adhesive}); in other words, for a specific adherend material, increasing the stiffness of adhesive base results in higher stress reduction in adhesive layer. Additionally, for a specific adhesive material, adherends with lower stiffness result in higher stress reduction in adhesive layer and consequently higher joint strength.

The failure load improvements reported in this research are related to the adherend and adhesive types which are used here. Further researches can be conducted to evaluate the effect of adhesive ductility on the efficiency of the non-flat adhesive joints. A number of researchers investigated the 3D stress state in different geometries of notched components considering constraint factors and stress concentration factors throughout the specimen thickness [46]. The main features of the in-plane stress distributions and the variability of the stress concentration factor as a function of the plate thickness were investigated in numerous researches [47-49]. The same methodology can be considered for the non-flat adhesive joints in order to evaluate the effect of adherends thickness on the mechanical behavior of components.

5. Conclusion

In the present project, the effect of non-flat interfaces as a method of joint strength improvement, was investigated experimentally and numerically. In the experimental part of the research, single lap joints with five different sinusoid interface profiles were created from aluminum alloy 7075-T6. The experimental results revealed that there are considerable differences between the load bearing capacity of bonded joints with different interface profiles. For the best cases, the joint strength of sinusoid SLJs was improved by 51% compared to the conventional single lap joint. As an important factor for investigating the strength of the adhesive joint, stress distribution of the adhesive layer was studied for different morphologies of adherend interfaces. Extensive parametric studies were carried out to highlight the role of interface shape and adherend/adhesive materials on the distribution of stresses in a bonded joint.

References

[1] P. Lazzarin, F. Berto, D. Radaj, Fatigue-relevant stress field parameters of welded lap joints: pointed slit tip compared with keyhole notch, Fatigue Fract. Eng. Mater. Struct. 32 (2009) 713-735.

[2] D. Radaj, P. Lazzarin, F. Berto, Fatigue assessment of welded joints under slit-parallel loading based on strain energy density or notch rounding, Int. J. Fatigue 31 (2009) 1490-1504.

[3] R. Jones, L. Molent, S. Pitt, Understanding crack growth in fuselage lap joints, Theor. Appl. Fract. Mech. 49(1) (2008) 38-50.

[4] L. Minnetyan, C.C. Chamis, Progressive fracture of adhesively bonded composite structures, Theor. Appl. Fract. Mech. 31(1) (1999) 75-84.

[5] V. Anes, R. Pedro, E. Henriques, M. Freitas, L. Reis, Bonded joints of dissimilar adherends at very low temperatures - An adhesive selection approach, Theor. Appl. Fract. Mech. 85 (2016) 99-112.

[6] P.N.B. Reis, J.R.L. Soares, A.M. Pereira, J.A.M. Ferreira, Effect of adherends and environment on static and transverse impact response of adhesive lap joints, Theor. Appl. Fract. Mech. 80 (2015) 79-86.

[7] P.A. Cooper, J.W. Sawyer, A critical examination of stresses in an elastic single lap joint, NASA Technical paper 1507, 1979.

[8] L. Tong, G.P. Steven, Analysis and design of structural bonded joints. Springer US, ISBN 978-0-7923-8494-6, 1999.

[9] M.R. Ayatollahi, M. Samari, S.M.J. Razavi, L.F.M. da Silva, Fatigue performance of adhesively bonded single lap joints with non-flat sinusoidal interfaces, Fatigue Fract. Eng. Mater. Struct. (In press) (DOI: 10.1111/ffe.12575)

[10] K. Gültekin, S. Akpinar, A. Özel, The Effect of Moment and Flexural Rigidity of Adherend on the Strength of Adhesively Bonded Single Lap Joints, J. Adhes. 91 (2014) 637-650.

[11] M.R. Ayatollahi, A. Nemati Giv, S.M.J. Razavi, H. Khoramishad, Mechanical properties of adhesively single lap bonded joints reinforced with multi-walled carbon nanotubes and silica nanoparticles. J. Adhes. (In press).

[12] H. Khoramishad, S.M.J. Razavi, Metallic fiber-reinforced adhesively bonded joints, Int. J. Adhes. Adhes. 55 (2014) 114–122.

[13] T. Okamatsu, M. Kitajima, H. Hanazawa, M. Ochi, Effect of modified silicone elastomer particles on the toughening of epoxy resin, J. Adhes. Sci. Technol. 12(8) (1998) 813-830.

[14] A. Buchman, H. Dodiuk-Kenig, A. Dotan, R. Tenne, S. Kenig, Toughening of epoxy adhesives by nanoparticles, J. Adhes. Sci. Technol. 23(5) (2009) 753-768.

[15] H. Kishi, K. Uesawa, S. Matsuda, A. Murakami, Adhesive strength and mechanisms of epoxy resins toughened with pre-formed thermoplastic polymer particles, J. Adhes. Sci. Technol. 19(15) (2005) 1277-1290.

[16] I.A. Akpinar, K. Gültekin, S. Akpinar, A. Gürses, A. Özel, An Experimental Study on Composite Adhesives Reinforced with Different Types of Organo-Clays, J. Adhes. (In press).

[17] E. Esmaeili, S.M.J. Razavi, M. Bayat, F. Berto, On the flexural behavior of metallic fiber reinforced adhesively bonded single lap joints, J. Adhes. (in press). (DOI: 10.1080/00218464.2017.1285235)

[18] M.R. Ayatollahi, A. Nemati Giv, S.M.J. Razavi, H. Khoramishad, The Effect of orientations of metal macrofiber reinforcements on the mechanical properties of adhesively bonded single lap joints, J. Adhes. (in press). (DOI: 10.1080/00218464.2017.1305270)

[19] C. Wang, J. Wang, T. Su, Determination of Water Diffusion Coefficients and Dynamics in Adhesive/Carbon Fiber–Reinforced Phenolic Resin Composite Joints, J. Adhes. 83(3) (2007) 255-265.

[20] W. Zielecji, A. Kubit, R. Kluz, T. Trzepiecinski, Investigating the influence of the chamfer and fillet on the high-cyclic fatigue strength of adhesive joints of steel parts, J. Adhes. Sci. Technol. (In press).

[21] A. Objois, B. Fargette, Y. Gilibert, The influence of the bevel angle on the micro-mechanical behaviour of bonded scarf joints, J. Adhes. Sci. Technol. 14(8) (2000) 1057-1070.

[22] H. Aglan, Z. Abdo, S. Shroff, Fracture and fatigue behavior of scrim cloth adhesively bonded joints with and without rivet holes, J. Adhes. Sci. Technol. 9(2) (1995) 177-197.

[23] J.N. Boss, V.K. Ganesh, C.T. Lim, Modulus grading versus geometrical grading of composite adherends in single-lap bonded joints, Compos. Struct. 62(21) (2003) 113-121.

[24] A.S. McLaren, I. Maclnnes, The influence on the stress distribution in an adhesive lap joint of bending of the adhering sheets, Br. J. Appl. Physics. 9(2) (1958) 72-77.

[25] G. Fessel, J.G. Broughton, N.A. Fellows, J.F. Durodola, A.R. Hutchinson, A numerical and experimental study on reverse-bent joints for composite substrates, 48th AIAA/ASME/ASCE/AHS/ASC Structures, Structural Dynamics, and Materials Conference, Honolulu, Hawaii, 2007.

[26] G. Fessel, J.G. Broughton, N.A. Fellows, J.F. Durodola, A.R. Hutchinson, Fatigue performance of metallic reverse-bent joints, Fatigue Fract. Engng. Mater. Struct. 32 (2009) 704–712.

[27] R.D.S.G. Campilho, A.M.G. Pinto, M.D. Banea, R.F. Silva, L.F.M. da Silva, Strength Improvement of Adhesively-Bonded Joints Using a Reverse-Bent Geometry, J. Adhes. Sci. Technol. 25(18) (2001) 2351–2368.

[28] M. You, Z. Li, X. Zheng, S. Yu, G. Li, D. Sun, A numerical and experimental study of preformed angle in the lap zone on adhesively bonded steel single lap joint, Int. J. Adhes. Adhes. 29 (2009) 280–285.

[29] Q. Zeng, C.T. Sun, A new bonded composite wavy lap joint, 41st AIAA/ASME/ASCE/AHS/ASC Structures, Structural Dynamics, and Material Conference, Atlanta, Georgia, US, 2000.

[30] Q. Zeng, C.T. Sun, Novel design of a bonded lap joint, AIAA J. 39(10) (2001) 1991–1996.

[31] Q. Zeng, C.T. Sun, Fatigue performance of a bonded wavy composite lap joint, Fatigue Fract. Eng. Mater. Struct. 27 (2004) 413–422.

[32] Q. Zeng, C.T. Sun, Fatigue performance of a bonded wavy composite lap joint, 42nd AIAA/ASME/ASCE/AHS/ASC Structures, Structural Dynamics, and Material Conference, Seattle, Washington, US, 2001.

[33] A.F. Avila, P.O. Bueno, Stress analysis on a wavy-lap bonded joint for composites, Int. J. Adhes. Adhes. 24(5) (2004) 407-414.

[34] G.S. Shiva Shankar, S. Vijayarangan, N.S. Krishna, Failure analysis of lap and wavy-lap composite bonded joints, Proceedings of the international symposium of research students on materials science and engineering, 2004, p. 1–8.

[35] G. Fessel, J.G. Broughton, N.A. Fellow, J.F. Durodola, A.R. Hutchinson, Evaluation of different lap-shear joint geometries for automotive applications, Int. J. Adhes. Adhes. 27(7) (2007) 574-583.

[36] P.I.F. Niem, T.L. Lau, K.M. Kwan, The effect of surface characteristics of polymeric materials on the strength of bonded joints, J. Adhes. Sci. Technol. 10 (1996) 361–372.

[37] L. Zhu, Y. Guan, Y. Wang, Z. Xie, J. Lin, J. Zhai, Influence of process parameters of ultrasonic shot peening on surface roughness and hydrophilicity of pure titanium, Surf. Coat. Technol. 317 (2017) 38-53.

[38] B.C. Rincon Troconis, G.S. Frankel, Effect of Roughness and Surface Topography on Adhesion of PVB to AA2024-T3 using the Blister Test, Surf. Coat. Technol. 236 (2013) 531-539.

[39] J.A. Juarez-Moreno, A. Avila-Ortega, A.I. Oliva, F. Aviles, J.V. Cauich-Rodriguez, Effect of wettability and surface roughness on the adhesion properties of collagen on PDMS films treated by capacitively coupled oxygen plasma, Appl. Surf. Sci. 349 (2015) 763-773.

[40] M. Ashrafi, A. Ajdari, N. Rahbar, J. Papadopoulos, H. Nayeb-Hashemi, A. Vaziri, Adhesively bonded single lap joints with non-flat interfaces, Int. J. Adhes. Adhes. 32 (2012) 46–52.

[41] S.M.J. Razavi, E. Esmaeili, M. Samari, S.M.R. Razavi, Stress analysis on a non-flat interface bonded joint, Journal of Adhesion. (In Press) (DOI:10.1080/00218464.2016.1257942)

[42] ASTM E8 / E8M-15a, Standard Test Methods for Tension Testing of Metallic Materials, ASTM International, West Conshohocken, PA, 2015.

[43] ASTM D638-14, Standard Test Method for Tensile Properties of Plastics, ASTM International, West Conshohocken, PA, 2014.

[44] German Institute for standardization (DIN). DIN 53281: Testing of adhesively bonded joints-Preparation of test specimens. Berlin: German standard; 2006.

[45] A. Boresi, R. Schmidt, Advanced mechanics of materials. John Wiley & Sons, 2003.

[46] A. Kotousov, P. Lazzarin, F. Berto, L.P. Pook, Three-dimensional stress states at crack tip induced by shear and anti-plane loading, Eng. Fract. Mech. 108 (2013) 65-74.

[47] F. Berto, A. Kotousov, P. Lazzarin, L.P. Pook, On scale effect in plates weakened by rounded V-notches and subjected to in-plane shear loading, Int. J . Fract. 180 (2013) 111-118.

[48] L.P. Pook, A. Campagnolo, F. Berto, P. Lazzarin, Coupled fracture mode of a cracked plate under anti-plane loading, Eng. Fract. Mech. 134 (2015) 391-403.

[49] F. Berto, P. Lazzarin, A. Kotousov, L.P. Pook, Induced out-of-plane mode at the tip of blunt lateral notches and holes under in-plane shear loading, Fatigue Fract. Eng. Mater. Struct. 35 (2012) 538-555.

Table captions

Table 1. The mechanical properties of the adherends and adhesive base.

Table 2. The composition of etching solution for aluminum alloys adherends [28].

Table 3. Details of finite element modeling of SLJs with sinusoid interface (A/H = 0.3, t = 0.2 mm).

Table 4. Details of finite element modeling of SLJs with sinusoid interface (wave length = $L/2$, t = 0.2 mm).

Table 5. Comparative numerical results of sinusoid SLJs with various adhesive thickness (wave length = $L/2$, A/H = 0.3).

Table 6. Comparative numerical results of sinusoid SLJs with various adherend materials (wave length = $L/2$, A/H = 0.3).

Figure captions

Fig. 1. Schematic view of modified single lap joints; (a) Reverse-bent SLJ, (b) wavy SLJ, (c) SLJ with sinusoid interface.

Fig. 2. Stress-strain curves of (a) 7075-T6 aluminum alloy, (b) Araldite® 2015 adhesive.

Fig. 3. The geometry of the adhesive joint.

Fig. 4. The flat and non-flat aluminum substrates prepared for applying the adhesive material.

Fig. 5. Schematic view of the gap between two adherends.

Fig. 6. The finite element models of sinusoid SLJs with different wave lengths and wave slope signs.

Fig. 7. The finite element model meshing used for stress analysis.

Fig. 8. Horizontal compressive and tensile stress distributions for the non-flat SLJs with negative and positive bond slope.

Fig. 9: (a) Load–displacement curves of single lap joints with sinusoid and flat interfaces. (b) Crack initiation and propagation at different stages of the experiments annotated with numbered 'events' in (a). The bold lines show undamaged regions of adhesive layer at each stage of deformation.

Fig. 10. Failure loads of the single lap joints with different interface geometries

Fig. 11. Peel stress distribution along the bond length for different sinusoid interface.

Fig. 12: Shear stress distribution along the bond length for different sinusoid interface.

Fig. 13. Peel stress distribution along the bond length for different wave heights.

Fig. 14. Shear stress distribution along the bond length for different wave heights.

Table 1. The mechanical properties of the adherends and adhesive base.

Mechanical property	Araldite® 2015	Al 7075-T6
Elastic modulus, E [GPa]	2	70
Poisson's ratio, v	0.33*	0.33
Tensile yield strength, σ_y [MPa]	14.4	448
Tensile failure strength, σ_f [MPa]	24.9	527

* manufacturer's data

Table 2. The composition of etching solution for aluminum alloys adherends [44].

Ingredient	wt%
Sulfuric acid	27.5
Sodium dichromate	7.5
Deionized water	65

Table 3. Details of finite element modeling of SLJs with sinusoid interface (A/H = 0.3, t = 0.2 mm).

Specimen label	Interface symmetry	Maximum normalized peel stress	Peel stress reduction* (%)	Maximum normalized shear stress	Shear stress reduction* (%)
Flat	-	1.71	-	1.16	-
S(2*L*)-	Symmetric	2.37	-39	1.39	-20
S(2*L*)+	Symmetric	2.37	-39	1.39	-20
S(*L*)-	Antisymmetric	1.39	19	0.79	32
S(*L*)+	Antisymmetric	3.15	-84	1.52	-31
S(2*L*/3)-	Symmetric	3.95	-131	1.60	-38
S(2*L*/3)+	Symmetric	3.95	-131	1.60	-38
S(*L*/2)-	Antisymmetric	1.01	41	0.66	43
S(*L*/2)+	Antisymmetric	4.59	-168	1.58	-36
S(2*L*/5)-	Symmetric	5.86	-243	1.84	-59
S(2*L*/5)+	Symmetric	5.86	-243	1.84	-59
S(*L*/3)-	Antisymmetric	1.01	41	0.76	34
S(*L*/3)+	Antisymmetric	6.87	-302	1.92	-66

* Stress reduction = ((maximum normalized stress)$|_{\text{Flat joint}}$ – (maximum normalized stress)$|_{\text{Sinusoid joint}}$) / (maximum normalized stress)$|_{\text{Flat joint}}$ × 100

Table 4. Details of finite element modeling of SLJs with sinusoid interface (wave length = $L/2$, t = 0.2 mm).

Wave height, A/H	Maximum normalized peel stress	Peel stress reduction* (%)	Maximum normalized shear stress	Shear stress reduction* (%)
-0.6	1.09	36	0.67	42
-0.5	0.87	49	0.64	45
-0.3	1.01	41	0.66	43
-0.2	1.44	16	0.83	28
0.0 (Flat)	1.71	-	1.16	-
0.2	3.60	-111	1.46	-26
0.3	4.59	-168	1.58	-36
0.5	8.38	-390	2.66	-129
0.6	9.85	-476	2.64	-128

* Stress reduction = ((maximum normalized stress)$|_{\text{Flat joint}}$ − (maximum normalized stress)$|_{\text{Sinusoid joint}}$) / (maximum normalized stress)$|_{\text{Flat joint}}$ × 100

Table 5. Comparative numerical results of sinusoid SLJs with various adhesive thickness (wave length = $L/2$, A/H = 0.3).

Adhesive layer thickness, t (mm)	Flat		Non-flat		Stress reduction* (%)	
	$\sigma_n\|_{max}$	$\sigma_s\|_{max}$	$\sigma_n\|_{max}$	$\sigma_s\|_{max}$	$\sigma_n\|_{max}$	$\sigma_s\|_{max}$
0.1	2.47	1.58	1.35	0.84	45	47
0.2	1.71	1.16	1.01	0.66	41	43
0.5	1.09	0.80	0.74	0.53	32	34
1.0	0.81	0.62	0.62	0.45	23	27

* Stress reduction = ((maximum normalized stress)$|_{\text{Flat joint}}$ − (maximum normalized stress)$|_{\text{Sinusoid joint}}$) / (maximum normalized stress)$|_{\text{Flat joint}}$ × 100

Table 6. Comparative numerical results of sinusoid SLJs with various adherend materials (wave length = $L/2$, A/H = 0.3).

Stiffness ratio,	Flat		Non-flat		Stress reduction* (%)	
($E_{adherends}$ / $E_{adheive}$)	$\sigma_n\|_{max}$	$\sigma_s\|_{max}$	$\sigma_n\|_{max}$	$\sigma_s\|_{max}$	$\sigma_n\|_{max}$	$\sigma_s\|_{max}$
100	1.05	0.76	0.74	0.54	30	29
35	1.71	1.16	1.01	0.66	41	43
10	2.97	1.87	1.50	0.94	50	49
2.5	4.75	2.81	2.30	1.60	52	43

* Stress reduction = ((maximum normalized stress)$|_{Flat\ joint}$ − (maximum normalized stress)$|_{Sinusoid\ joint}$) / (maximum normalized stress)$|_{Flat\ joint}$ × 100

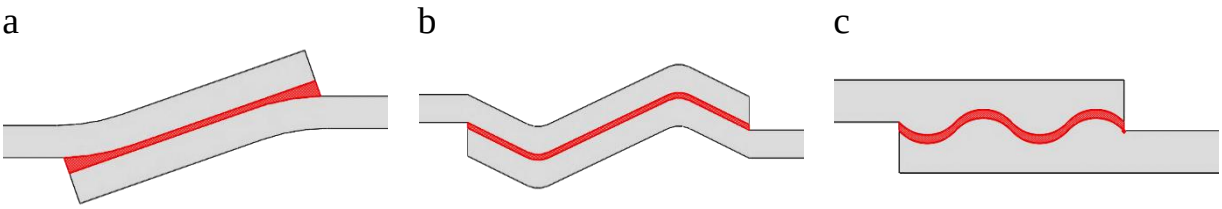

Fig. 1. Schematic view of modified single lap joints;
(a) Reverse-bent SLJ, (b) wavy SLJ, (c) SLJ with sinusoid interface.

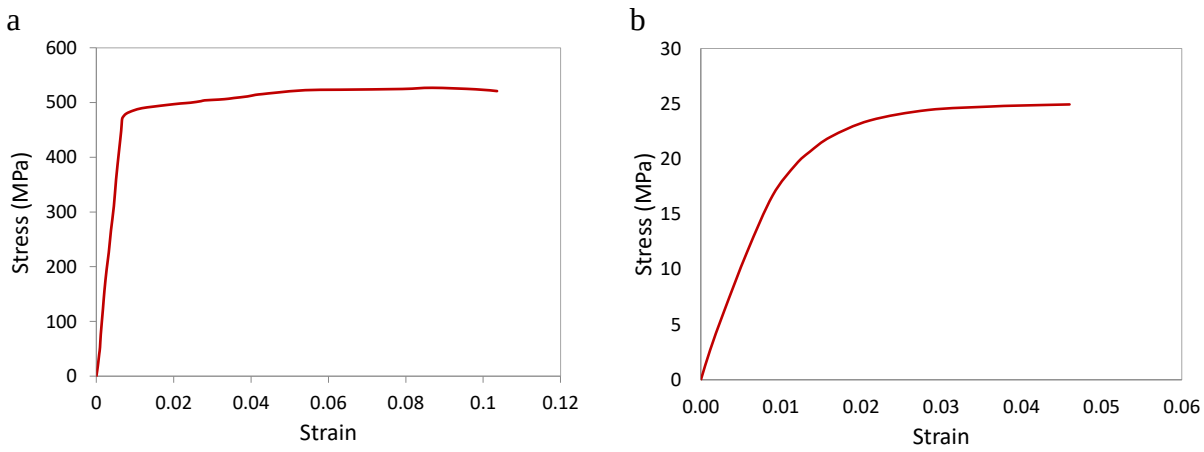

Fig. 2. Stress-strain curves of (a) 7075-T6 aluminum alloy, (b) Araldite® 2015 adhesive.

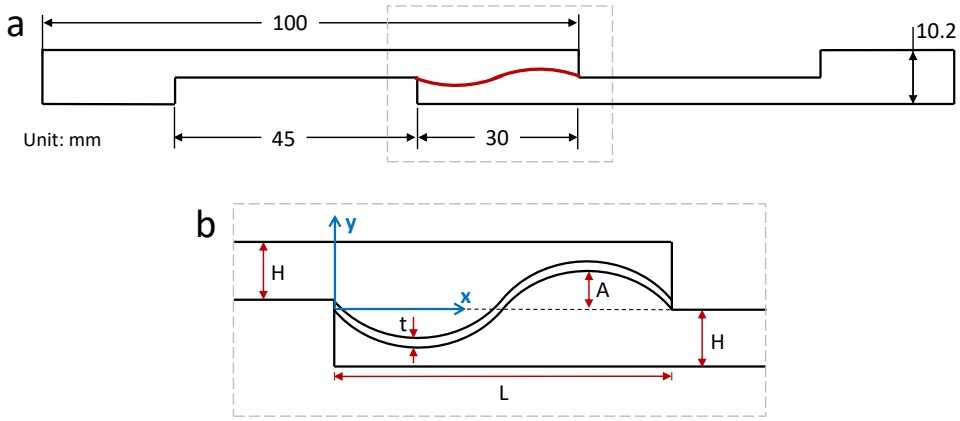

Fig. 3. The geometry of the adhesive joint.

Fig. 4. The flat and non-flat aluminum substrates prepared for applying the adhesive material.

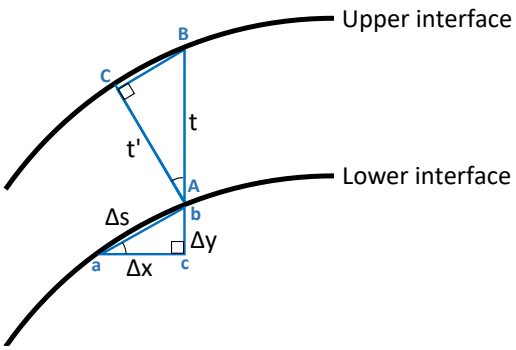

Fig. 5. Schematic view of the gap between two adherends.

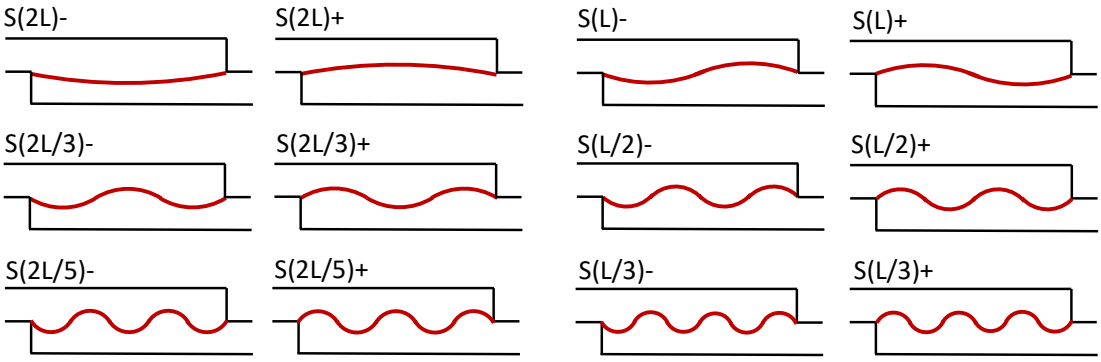

Fig. 6. The finite element models of sinusoid SLJs with different wave lengths and wave slope signs.

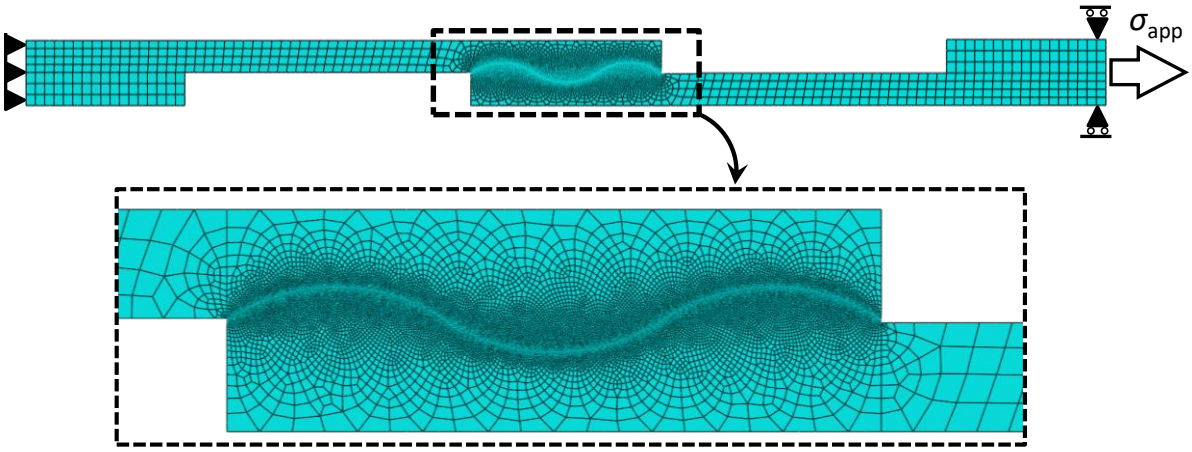

Fig. 7. The finite element model meshing used for stress analysis.

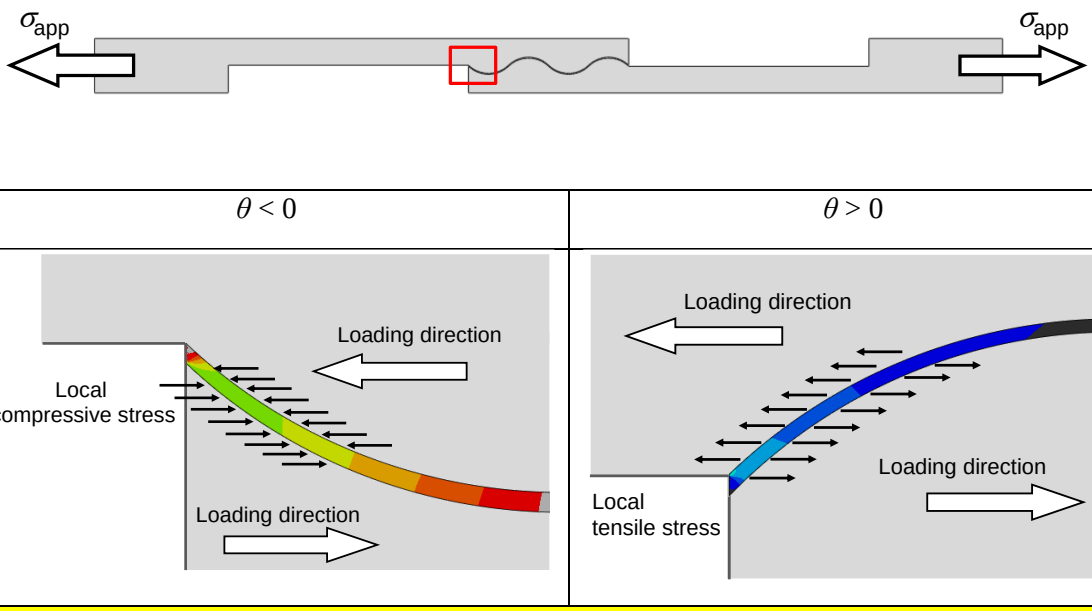

Fig. 8. Horizontal compressive and tensile stress distributions for the non-flat SLJs with negative and positive bond slope.

a

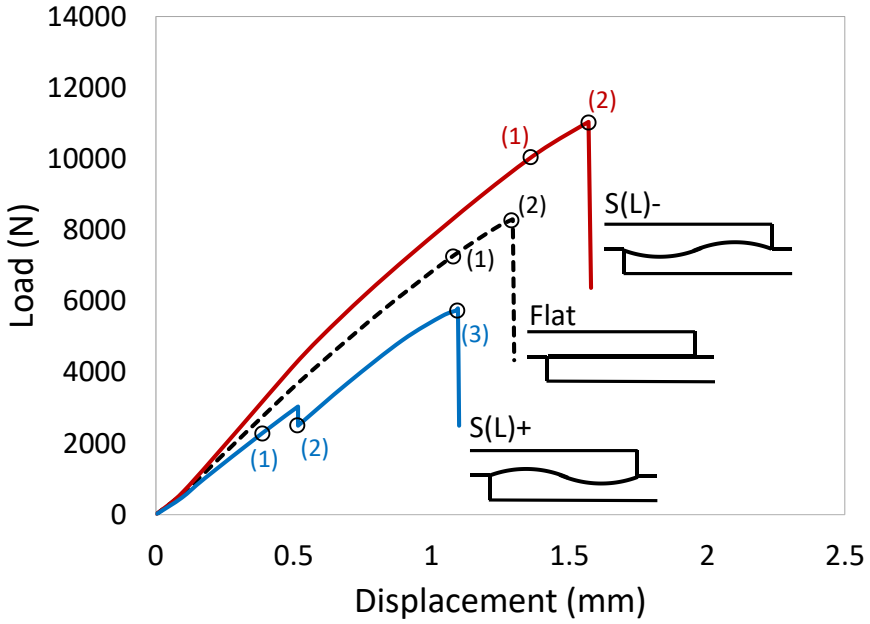
14000
12000
10000
8000
6000
4000
2000
0
Load (N)
0
0.5
1
1.5
2
2.5
Displacement (mm)
(1)
(2)
S(L)-
Flat
(3)
S(L)+

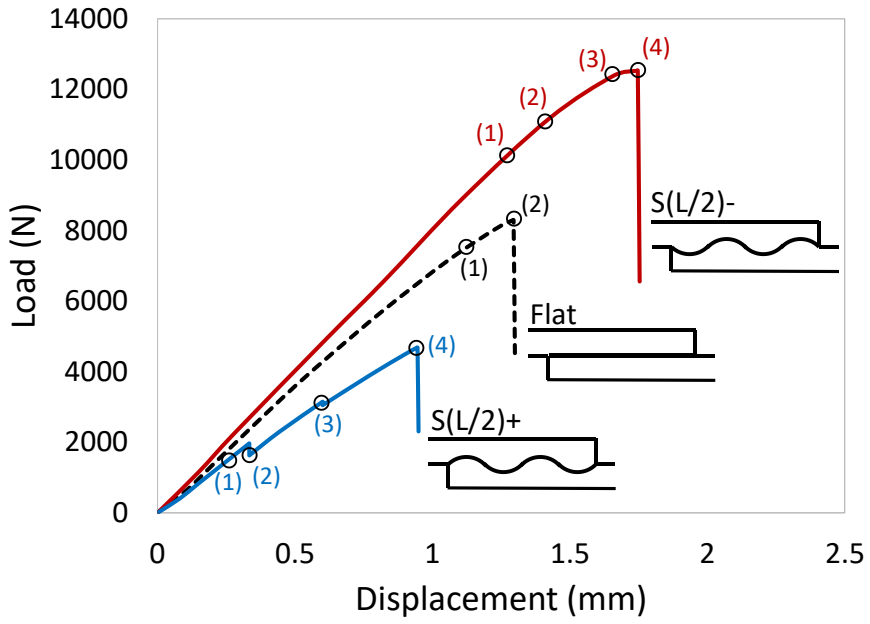
14000
12000
10000
8000
6000
4000
2000
0
Load (N)
0
0.5
1
1.5
2
2.5
Displacement (mm)
(1)
(2)
(3)
(4)
S(L/2)-
Flat
S(L/2)+

b

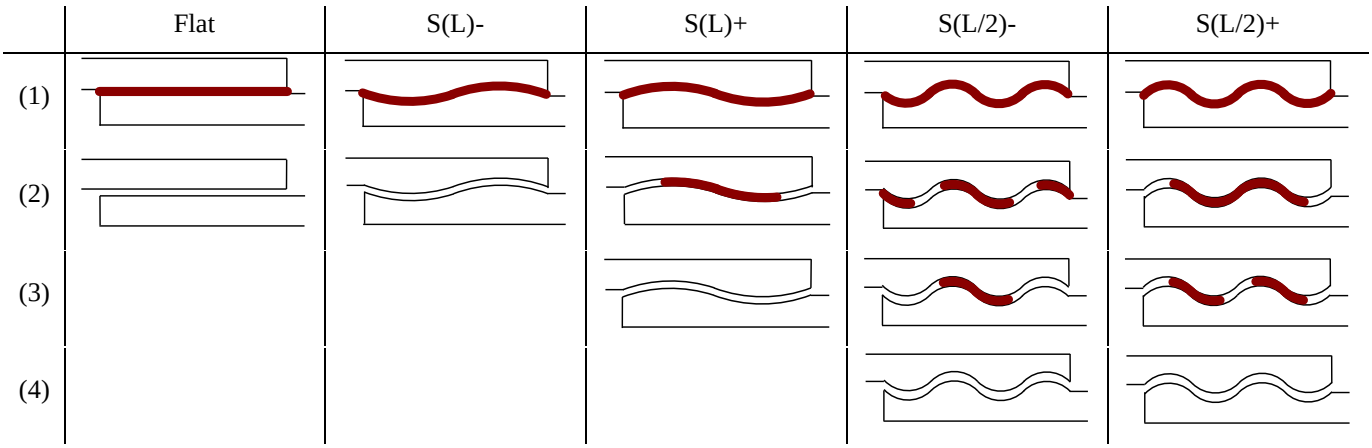

Fig. 9: (a) Load–displacement curves of single lap joints with sinusoid and flat interfaces. (b) Crack initiation and propagation at different stages of the experiments annotated with numbered ‘events’ in (a). The bold lines show undamaged regions of adhesive layer at each stage of deformation.

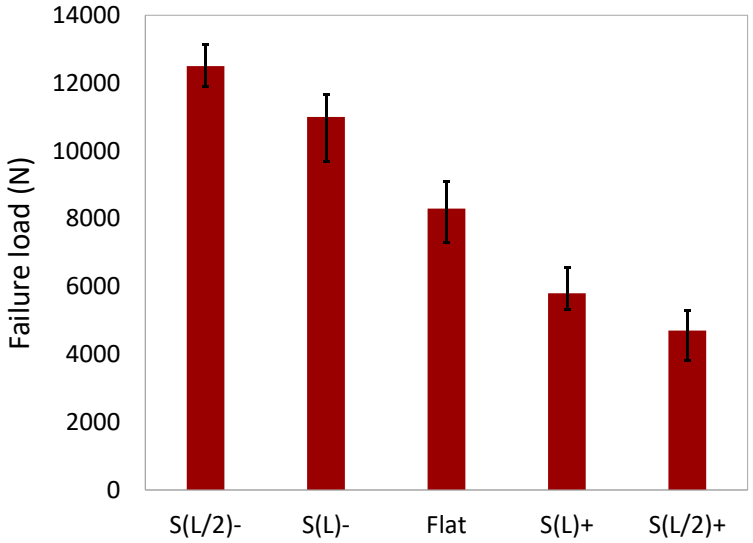

Fig. 10. Failure loads of the single lap joints with different interface geometries

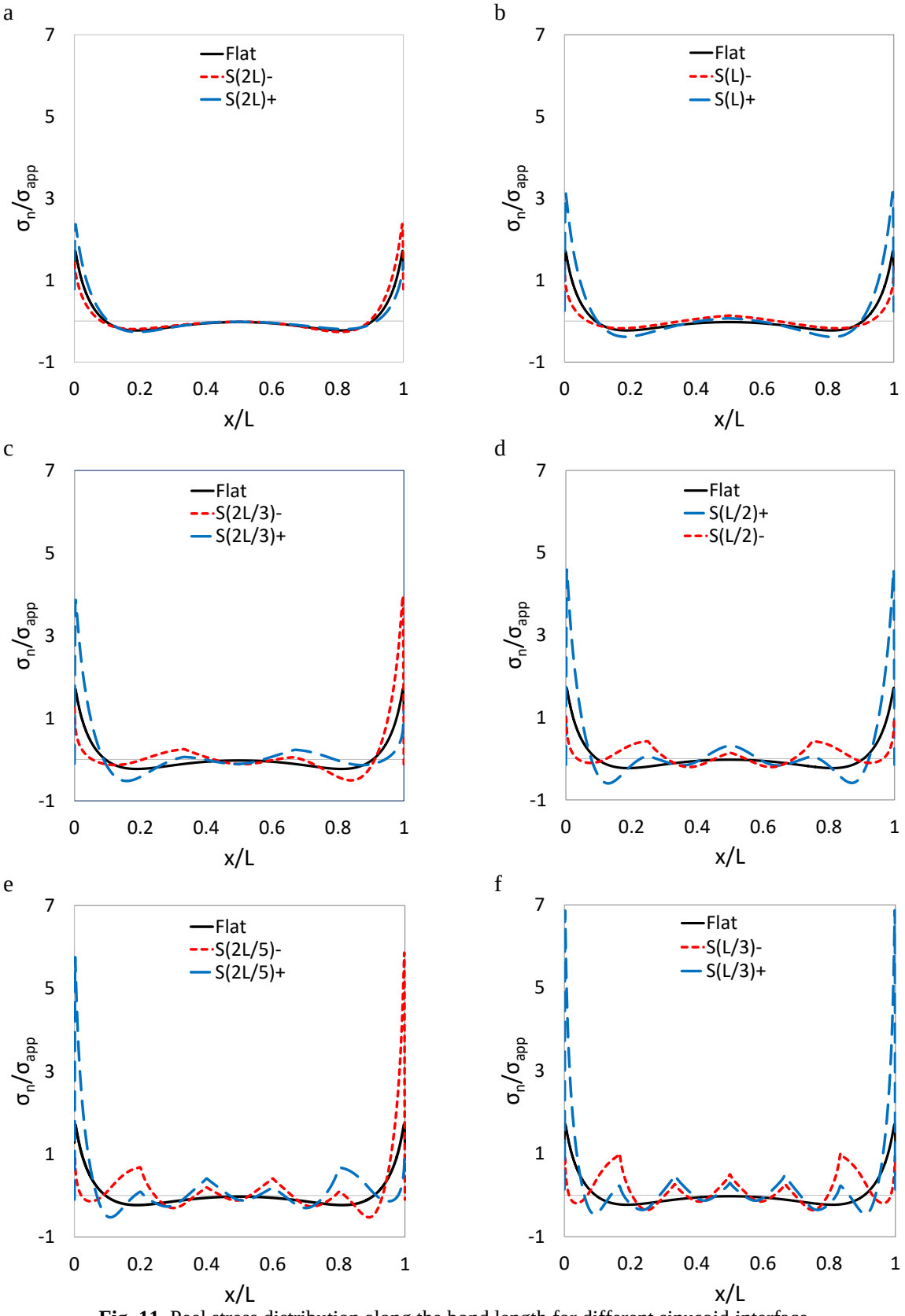

Fig. 11. Peel stress distribution along the bond length for different sinusoid interface.

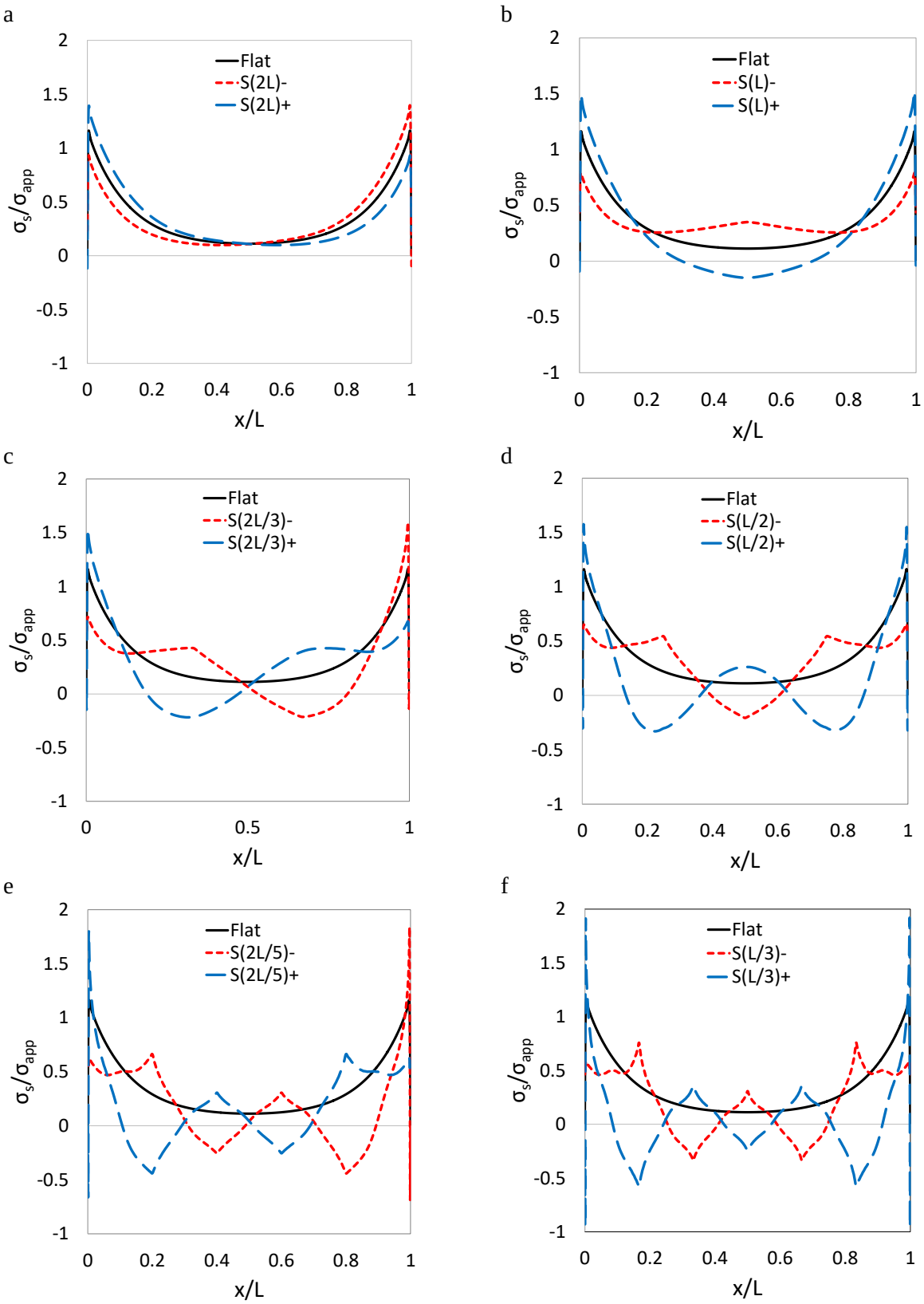

Fig. 12: Shear stress distribution along the bond length for different sinusoid interface.

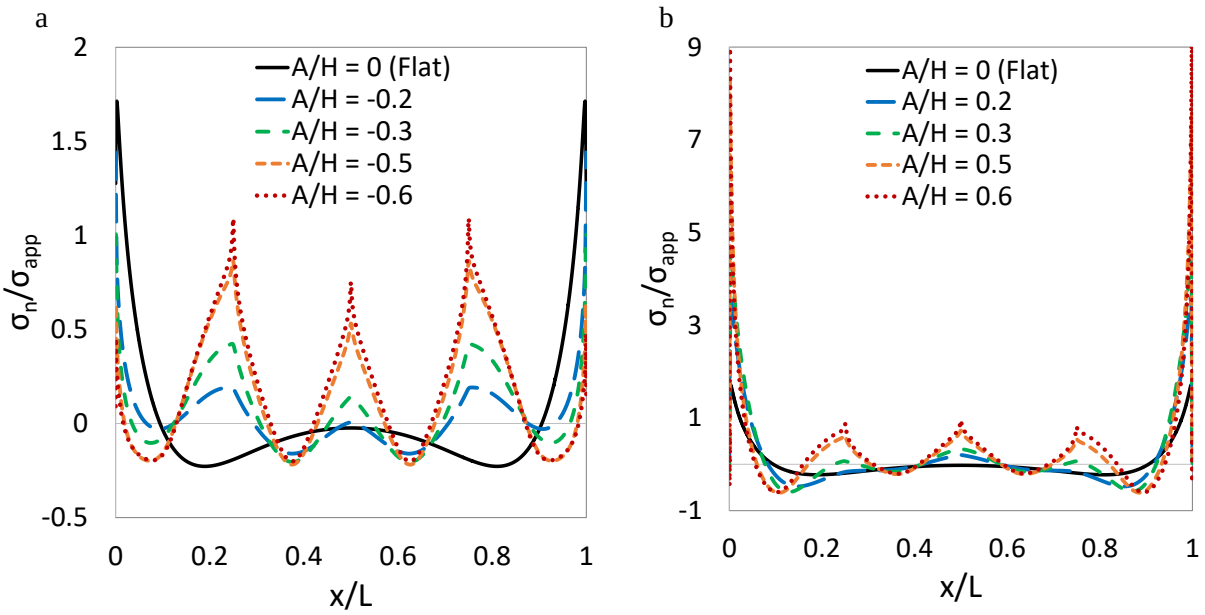

Fig. 13. Peel stress distribution along the bond length for different wave heights.

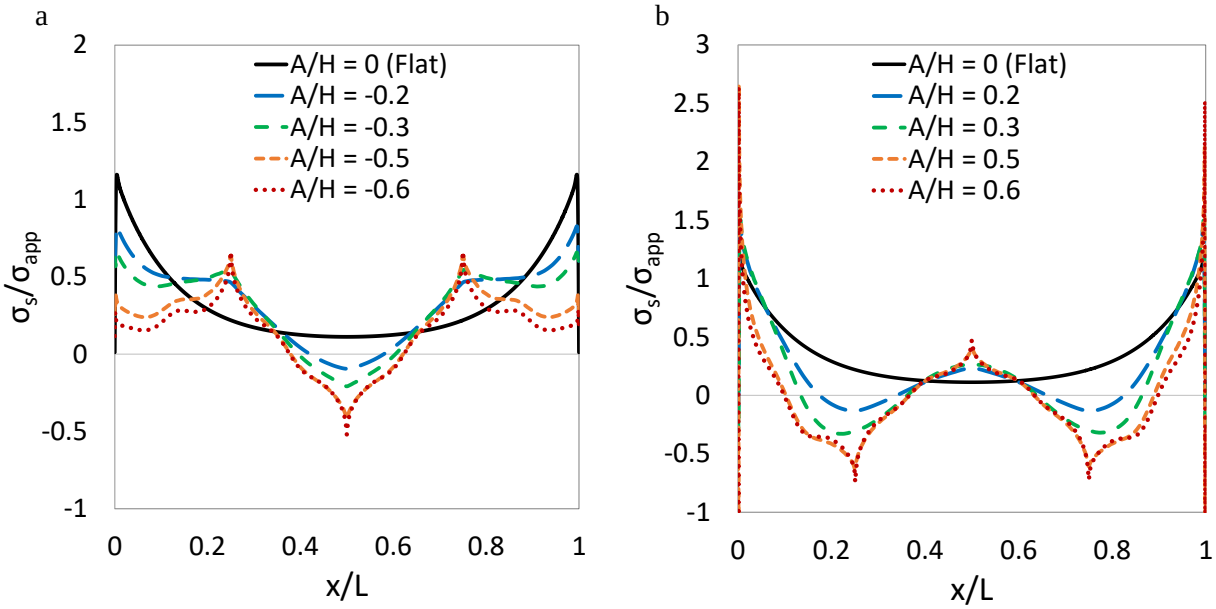

Fig. 14. Shear stress distribution along the bond length for different wave heights.